Modelling and Simulation in Materials Science and Engineering

PAPER

Atomistic study of crack-tip plasticity in precipitation hardened monocrystalline aluminum

IOP Publishing Modelling and Simulation in Materials Science and Engineering
Modelling Simul. Mater. Sci. Eng. **27** (2019) 065009 (18pp) https://doi.org/10.1088/1361-651X/ab20ae

Atomistic study of crack-tip plasticity in precipitation hardened monocrystalline aluminum

Thomas Berton[1] **and Chandra Veer Singh**[1,2]

[1] Department of Materials Science and Engineering, University of Toronto, 184 College Street, Toronto, ON, M5S 3E4, Canada
[2] Department of Mechanical and Industrial Engineering, University of Toronto, 5 King's College Road, Toronto, ON, M5S 3G8, Canada

E-mail: chandraveer.singh@utoronto.ca

Received 11 October 2018, revised 28 April 2019
Accepted for publication 9 May 2019
Published 6 June 2019

Abstract

Understanding the atomistic mechanisms of dislocation-based plasticity ahead of a crack-tip in precipitation hardened alloys is a challenging problem due to the complexity of the interactions between the precipitates in the microstructure and the variety of defects nucleated at the crack-tip, such as dislocations, stacking faults and micro-twins. In this paper, we use classical molecular dynamics simulations to perform a comprehensive atomistic analysis of the factors that influence the motion of dislocations ahead of a crack-tip in precipitation hardened aluminum. Specifically, the effects of planar copper GPII zones on the motion of dislocations emitted at the crack-tip of an aluminum crystal in four different crystal orientations under constant strain-rate loading were investigated. By placing the precipitates close to the crack-tip, it was found that they did not affect the nucleation of the first dislocation significantly unless they were located immediately ahead. Moreover, in some crystal orientations, subsequent nucleations were appreciably delayed due to the shielding effect of the first dislocation interacting with the precipitate. Following emission, the interaction between the emitted dislocations and the precipitates consisted of different mechanisms, including shear cutting, Orowan looping, and cross-slip, depending on the crystal orientation. The resistance to dislocation motion caused by the precipitates was quantified by determining the interaction time between each dislocation and the precipitates. It was found that although the applied load in each unit cell was high, the dislocations could be significantly slowed down in some of the crystals. This resulted in less dislocation activity ahead of the crack-tip, especially in the crystals for which micro-twinning was the dominant driver of plasticity. The

results of this work pave the way for the development of accurate models to predict the evolution of plasticity in metallic materials by providing a quantified assessment of dislocation motion in complex alloy microstructures.

Keywords: dislocation, precipitate, micro-twin, crack, molecular dynamics

(Some figures may appear in colour only in the online journal)

1. Introduction

Enhancing the strength of structural materials, without compromising with their ductility, formability and fracture toughness has been a long-held problem in materials engineering. While it is understood that precipitation hardening is an effective method for improving the strength of metallic materials, experimental findings [1, 2] have shown that it can lead to a reduction in ductility and fracture toughness, causing premature failure in practical applications.

The mechanism of fracture in metals and alloys starts at the atomistic scale, through a process of atomic debonding and crack nucleation. Following nucleation, a series of defects can be emitted from the crack-tip, such as dislocations and micro-twins, eventually leading to final failure. In order to understand atomic-level crack plasticity, several attempts have been made to gather insights into the governing mechanisms [3–24]. For example, Rice's theory of dislocation nucleation at a crack-tip has been used for predicting the nucleation of dislocations from crack-tips in metallic monocrystals with different crystal orientations [5, 6, 9, 11]. Researchers have also focused on understanding the mechanisms of crack propagation [10, 12, 14, 18], the interaction of the crack-tip with grain boundaries [7], and the effect of solutes on dislocation nucleation [11, 17]. Larger scale simulations have observed strain hardening around a cracked surface [8], and the growth of a crack lying across a twin boundary [3]. Nevertheless, although these studies have provided great insights into the mechanisms of crack growth in pure crystals, their applicability to metallic systems which are composed of precipitates is still limited because the interactions of the cracks with the microstructure have so far not been accounted for.

The interactions of dislocations with lattice obstacles have been studied using atomistic modeling, in order to understand the onset of plasticity in metallic alloys [7, 25–27]. Notably, Bacon and Osetsky [27] conducted a study on the interactions of dislocations with different types of lattice defects in BCC and FCC crystals. Singh and Warner [25, 28, 29] looked into the interactions between precipitates and dislocations and their effect on hardening for an AlCu system. They developed a multi-scale model capable of explaining the age-hardening curves of the AlCu alloy system. Theoretical models have also been developed for predicting the interactions between dislocations and solutes and their effect on dislocation flow stress [30–32]. These studies have allowed for more accurate predictions of the yielding behavior in metallic alloys. However, the understanding of post-yielding deformation processes following the nucleation of cracks in the microstructure in precipitation hardened alloys remains unclear. Towards this effort, two previous works have investigated the effect of precipitates on defect nucleation at a crack-tip. Machova *et al* [4] studied a BCC Cu rectangular precipitate in a cracked BCC Fe matrix and described the interaction mechanisms. Their work focused on a very specific type of precipitate that is created during nuclear irradiation, which causes material embrittlement. Liu and Groh [33], on the other hand, studied the interaction between a void and a crack in BCC Fe and evaluated the effects of temperature and void

position on crack-tip defect nucleation. Although these two last contributions have provided some insight into the interaction of crack-tip nucleated defects with lattice obstacles, to-date, there has been no comprehensive atomistic study of the effects of precipitates on crack-tip plasticity, and on the motion of crack-tip dislocations following their nucleation.

In order to understand crack-tip plasticity in age hardened alloys, four problems need to be addressed. First, the effect of realistic reinforcing precipitates on crack-tip dislocation nucleation has not yet been comprehensively studied at the atomistic level and it is not clear whether they inhibit or enhance nucleation. Second, it is not known whether precipitates affect the nature of the defect nucleated at the crack-tip. Yamakov *et al* [9] showed that crystal orientation dictated whether the defect nucleated at a crack-tip in aluminum was a full dislocation, or a micro-twin; however, it is possible that the precipitate may affect this competition through its influence on the local crack-tip stresses. Third, the interaction mechanisms between a dislocation moving in the stress field of a sharp crack and a precipitate have not been fully investigated either. This is a new problem because, in cracked systems, the loading and boundary conditions for dislocation motion will be different than in systems where dislocations are already artificially included [25]. Cracks can also serve as the nucleation point for micro-twins, whose interactions with precipitates have not been studied comprehensively using atomistic modeling before. Fourth, in order to guide the development of sophisticated models of crack-tip plasticity, the effect of precipitates on the dynamics of dislocations around crack-tips needs to be quantified.

The current work aims to fill the gap in the current knowledge of plasticity mechanisms around crack-tips in precipitate hardened alloys. The system studied was an Al crystal with planar Cu Guinier-Preston II (GPII) zones located in the vicinity of the crack-tip, which are known to significantly reinforce Al structural alloys. We have examined the effect of GP zones on dislocation nucleation, and the subsequent interaction of the dislocations with the GP zones. The effect of the precipitate on the distribution of stresses at the crack-tip has been assessed as well to explain the results. The results have been compared to previous theoretical and computational studies to validate the modeling approach. We have also examined the influence of crystal orientation on the interaction between the dislocation and the precipitate; in particular, by changing the crystal orientation, the effect of dislocation core structure on its interaction with the precipitate has been studied. Lastly, the dislocation activity has been quantified by monitoring the size of the plastic zone ahead of the crack-tip, and by determining the reinforcing effect of the precipitates relative to a pristine crystalline system. To our knowledge, this is the first in-depth atomistic study to comprehensively describe and quantify the mechanisms of dislocation-precipitate interaction in a cracked FCC crystal. The results point to the importance of atomistic insights for the development of multi-scale models of metallic alloy failure.

2. Methodology

Molecular Dynamics simulations were performed using the open-source program LAMMPS [34]. The system studied (see figure 1) was an Al single crystal, with a crack located on its side. A cartesian coordinate system was attached to the simulation cell, with the following approximate dimensions: 150 nm in the x direction, 150 nm in the y-direction, and 20 nm in the z (thickness) direction. The boundaries were set to be periodic in the z direction, and free in the x and y directions. Four different crystal orientations were studied, which are identified based on the plane of the crack, and the direction of the crack front. The orientations are provided in table 1. In all cases, the atomistically sharp crack was created by preventing

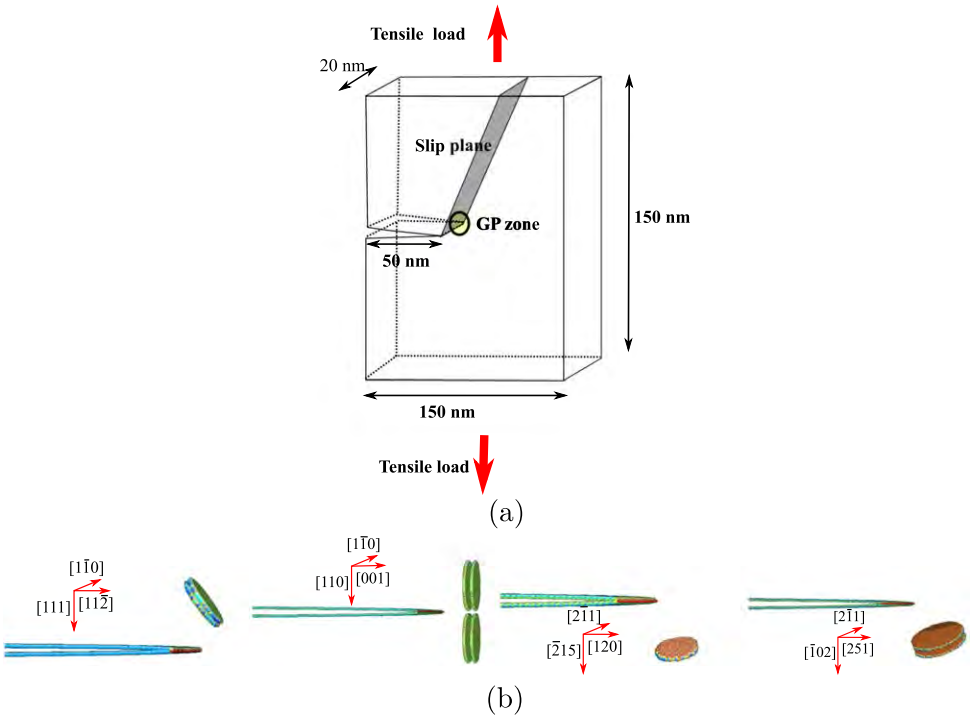

Figure 1. System geometry. A planar GP zone is placed on the slip plane, and periodic boundary conditions are applied across the thickness of the box. The top and bottom boundaries are fixed, while the left and right boundaries are free. 4 different crystal orientations have been studied. Crystal orientations (A–D) are provided; the GP zone is placed either 10 or 100 Å ahead of the crack-tip.

Table 1. Mechanical properties for the different crystal orientations, critical energy release rates, and stress intensity factors for dislocation nucleation.

	System label crystal orientation	A (111) [1$\bar{1}$0]	B (110) [1$\bar{1}$0]	C ($\bar{2}$15) [2$\bar{1}$1]	D ($\bar{1}$02) [2$\bar{1}$1]
	θ	70.53°	35.26°	50.77°	39.23°
	ϕ	0°	0°	30°	30°
	μ (GPa)	27	27	27	27
	ν	0.32	0.27	0.32	0.34
G_{Ie} (mJ m^{-2})	Rice model	1080	2116	1602	2205
	MD (ADP)	1210	914	787	1174
K_{Ie} (MPa m$^{-1/2}$)	MD (ADP)	0.31	0.26	0.25	0.31
	MD (EAM)[a]	0.26	0.24	0.21	0.28

[a] See [9].

inter-atomic interactions between both sides of the crack. The length of the crack was set to 50 nm to prevent the free boundaries on the left and the right of the simulation from affecting the distribution of stresses around the crack-tip. A Cu Gunier-Preston II (GPII) zone was

introduced onto the slip plane of the crystal that contained the crack front, approximately 100 Å from the crack-tip. In some simulations, the precipitate was placed at 10 Å from the crack-tip. The diameter of the precipitates was set to 10 nm. The precipitates in most simulations consisted of two layers of Cu atoms separated by three atomic planes of Al. The two Cu layers lay in the {100} family of planes. This particular type of precipitate was chosen because it is commonly found in age hardened aluminum, and provides significant reinforcement by pinning dislocations [35]. In one simulation case, a smaller GPI zone of 6 nm in diameter was used, as the results for a 10 nm precipitate were inaccurate.

In general, the EAM potential developed by Ye and Cai [36], and the angular-dependent potential (ADP) developed by Apostol and Mishin [37] are used for the MD simulations of AlCu systems. The ADP has been reported to predict accurate thermodynamic properties for the different phases of the AlCu system [37]. Moreover, it has been used by Singh and Warner [25, 28] to successfully model the hardening effects of precipitates in the AlCu alloy system. It also more accurately models the stacking fault energy curve, and therefore can better represent plastic behavior in AlCu. Therefore, we used the ADP for the simulations. The energy of a system described by the ADP is given by the following expression:

$$E_{\text{tot}} = \frac{1}{2}\sum_{i,j(j\neq i)} \Phi_{s_i s_j}(r_{ij}) + \sum_i F_{s_i}(\bar{\rho}_i) + \frac{1}{2}\sum_{i,\alpha}(\mu_i^{\alpha})^2 + \frac{1}{2}\sum_{i,\alpha,\beta}(\lambda_i^{\alpha\beta})^2 - \frac{1}{6}\sum_i \nu_i^2, \tag{1}$$

where $\Phi_{s_i s_j}$ is the pair-interaction potential and $F_{s_i}(\bar{\rho}_i)$ is the embedding energy of atom i with the electron density $\bar{\rho}_i$. The first two terms on the right-hand side of equation (1) correspond to the EAM formulation. The last three terms represent angular effects through dipole and quadrupole parameters, which favor a cubic crystal structure. The crystal orientations studied in this paper are provided in table 1.

We used a simulation timestep of 1 fs to integrate the equations of motion. At first, an energy minimization based on the conjugate gradient method was performed. Next, the temperature was initialized at 0.01 K and the system was equilibrated at that temperature for 10 picoseconds, and the simulations were conducted in this minimum energy regime to study stress-mediated mechanisms of plasticity. The simulation box was subsequently strained by adding a velocity to the atoms in the y-direction. Free boundary conditions were used on the sides of the box. The velocity was ramped from 0 at the bottom of the box to its maximum value at the top of the box in order to simulate tensile deformation. The velocities of the atoms in the simulation box were set so that the total strain rate applied to the simulation box was equal to $10^8\ \text{s}^{-1}$. The forces on the atoms at the top and bottom boundaries were set to 0. Following defect nucleation at the crack-tip after a certain amount of applied strain, results were visualized using AtomEye [38], and the common neighbor analysis tool [39]. There was a negligible increase in temperature as dislocations were emitted. Dislocations were analyzed with a recently developed method, the dislocation extraction algorithm [40], that allowed for identification of the Burgers vector.

3. Results and discussion

3.1. Effect of crystal size

Atomistic simulations of crack-tip plasticity require a sufficiently large crystal in order to adequately represent the distribution of stresses ahead of the crack-tip. As discussed by Moller [22], in atomistic systems of a few million atoms, the stress distribution ahead of the crack-tip in an atomistic system can be described using Linear Elastic Fracture Mechanics

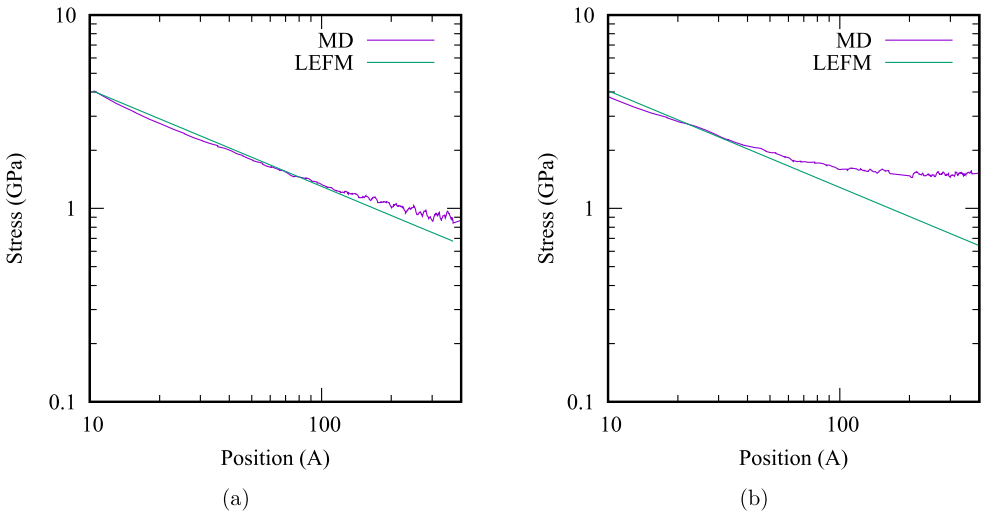

Figure 2. Distribution of stress (σ_{yy}) in: (a) a crystal with a large crack and (b) a crystal with a small crack at 1.05% strain. Crystal orientation B: (110)[1$\bar{1}$0].

(LEFM) for atoms within a small distance of the crack-tip, while boundary effects start dominating as one moves closer to the free edges of the simulation cell. Therefore, in order to accurately account for the effects of precipitates on the motion of dislocations in the vicinity of the crack-tip, the precipitates should be sufficiently close to the crack. The effect of crystal dimensions was studied by first creating a large system, with dimensions described in section 2 of this paper, and a small system with lateral dimensions 75 nm $\times$ 75 nm, with a smaller crack of length 25 nm. The crystal orientation is denoted as (110)[1$\bar{1}$0], where the plane of the crack and the direction of the crack front are indicated. This corresponds to crystal orientation B considered in this paper.

In figure 2, the stress distribution ahead of the crack-tip has been plotted for the two crystal sizes, at 1.05% strain. There are two curves in each plot: the stress evolution without a precipitate obtained from MD simulations, and the stress evolution expected from LEFM. Note that the stress profiles were plotted prior to dislocation nucleation and the onset of plastic deformation. The analytical stress distribution was obtained from LEFM by assuming that aluminum could be modeled using linear isotropic elasticity theory. Accordingly, the stress distribution ahead of the crack-tip in the vertical (σ_{yy}) direction is given as follows:

$$\sigma_{yy} = \frac{K_I}{\sqrt{2\pi r}} \cos\left(\frac{\theta}{2}\right)\left[1 + \sin\left(\frac{\theta}{2}\right)\sin\left(\frac{3\theta}{2}\right)\right], \tag{2}$$

where K_I is the stress intensity factor, r is the distance from the crack-tip, and θ is the angular coordinate with respect to the plane of the crack. K_I was obtained by calculating stresses in a region ahead of the crack-tip, and fitting this distribution to the analytical expression shown above. Then, based on the calculated value of K_I, the stress distribution along the slip plane of the crystal (oriented at 35.26° with respect to the plane of the crack) was plotted using equation (2).

Inspection of figure 2 shows that for both crystal sizes, the stress distribution is in good agreement with LEFM up to a short distance ahead of the crack-tip: approximately 100 Å for the larger crystal, and 50 Å for the small crystal. Past this small distance, the stress (σ_{yy}) is constant, and corresponds to the average stress in the simulation cell; this convergence in

stress is due to the free boundary conditions used for the sides of the box. Therefore, these results suggest that in order to optimize the accuracy of the simulations, the crystal with a larger crack should be used. In the remainder of this paper, the effect of crystal size on the results will be discussed in order to ascertain the validity of the current analysis for realistic macroscopic systems.

In figure 3, the atomistic stress profile for σ_{yy} has been plotted for crystal orientations A to D to show the effect of the crack-tip on the stress distribution around the precipitate. The applied strain is 1.1%, at which point the deformation is purely elastic, and no dislocation has been nucleated from the crack-tip. In the absence of a precipitate, the stress distribution is in agreement with LEFM for linear elastic materials close to the crack-tip. Further away from the crack-tip, the stress is constant due to the boundary conditions applied to the simulation cell. When a precipitate zone is placed on one of the slip planes 100 Å ahead of the crack-tip, it is clear that in all four crystal orientations, the stress field around the precipitate is significantly affected by the crack-tip environment. In the case of crystal orientation A, the misfit stress field induced by the precipitate's different lattice constant leads to a complex combination of tensile and compressive stresses (σ_{yy} component of the stress tensor). The precipitate is mostly under a state of tension due to its lower lattice constant relative to Al. In the case of crystal orientation D, the Cu layers are in fact under a state of compression. This is due to the orientation of the zone relative to the applied loading direction. These stress profiles show that the stress field induced around the precipitates is strongly dependent on which crystal orientation is considered, which might have an effect on the interaction of dislocations with the precipitates. Lastly, note that the precipitates are sufficiently close to the crack-tip that the stress fields would be representative of a macroscopic crack in a large plate.

3.2. Effect of precipitate on dislocation nucleation and emission

We now study the nucleation of dislocations from the crack-tip of the aluminum crystal, for all four crystal orientations. The initial length of the crack was 50 nm in all simulations. The critical stress intensity factors (K_{Ie}) for nucleation of the first dislocation for each of the four crystal orientations in the absence of a precipitate on the slip plane ahead of the crack-tip are provided in table 1. To obtain K_{Ie}, the atomic stress profile around the crack-tip was fit to analytical expressions [6] for stress distribution ahead of a crack (see equation (2)). We calculated the critical energy density release rate using Rice's model [23] of dislocation nucleation which expresses the critical energy density release rate for dislocation nucleation in terms of the unstable stacking fault energy γ_{usf}. The magnitude of γ_{usf} depends on the inter-atomic potential ($\gamma_{\text{usf}} = 160\ \text{mJ m}^{-2}$ for ADP [37], which was validated with separate calculations of the stacking fault energy curve). Due to the orientation of the crystal, where the slip plane of the dislocations is at an angle relative to the loading axis, the critical energy release rate G_{disl} is given by the following equation [23]:

$$G_{\text{disl}} = 8\gamma_{\text{usf}} \frac{1 + (1 - \nu)\tan^2(\phi)}{(1 + \cos(\theta))\sin^2(\theta)}, \tag{3}$$

where ν is Poisson's ratio, θ is the angle of the slip plane relative to the globally applied stress, and ϕ is the angle between the Burgers vector and the slip direction. These parameters are provided in table 1. On the other hand, the critical energy release rate obtained from LEFM and the MD simulations is given by:

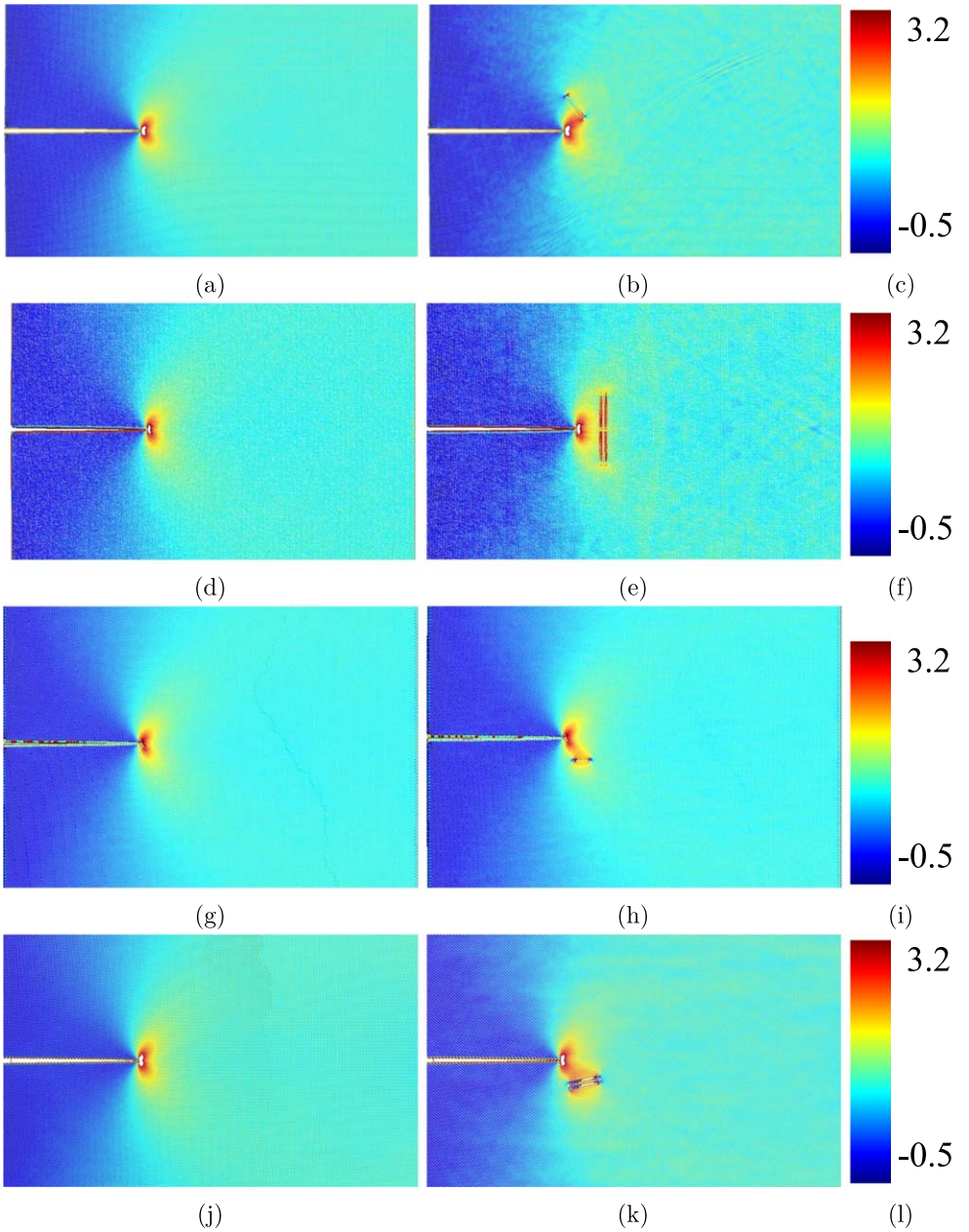

Figure 3. Stress distribution (σ_{yy}) in each crystal orientation (A to D), without and with a GP zone. The color bars are expressed in units of GPa, with negative values showing compressive stresses. Applied strain is 1.1% in both cases.

$$G_{Ie} = K_{Ie}^2 \frac{(1-\nu)}{2\mu}, \tag{4}$$

where μ is the shear modulus and K_{Ie} is the critical stress intensity factor for dislocation nucleation obtained from the atomistic simulations. The values of G_{Ie} are shown in table 1.

The plane of the crack is indicated inside brackets, and the direction of the crack front is shown inside square brackets. Additionally, in the same table, we report the results from a previous computational study [9] for comparison.

From table 1, we can see that the critical energy release rate G_{Ie} for the first crystal orientation predicted from Rice's model, and the results of the current simulations are close. However, the magnitudes of the critical energy release rates G_{Ie} obtained in the simulations for crystal orientations B ((110)[1$\bar{1}$0]), C (($\bar{2}$15)[2$\bar{1}$1]) and D (($\bar{1}$02)[2$\bar{1}$1]) are significantly smaller than the predictions from Rice's theory. This discrepancy could be due to the tension-shear coupling effect (as discussed by Cheng *et al* [5]), where the nucleation of a dislocation is easier when the adjacent {111} planes ahead of the crack are separated by a larger distance than at equilibrium, which had not been considered in Rice's theory. These discrepancies between the simulation results and Rice's model have been observed in other atomistic studies [41]. From table 1, we can see that the results reported in [9] are slightly smaller than the ones reported here. This behavior could be due to the difference in simulation temperatures, since the results reported in [9] are for a temperature of 300 K, whereas current results correspond to a temperature of 0.01 K. Nucleation of dislocations is a thermally activated process, therefore its probability increases as the temperature of the system is increased. Additionally, a larger temperature leads to a lower unstable stacking fault energy γ_{usf}, thereby decreasing the critical energy release rate required for the nucleation. We note that these results show that both the EAM potential used by Yamakov *et al* and the ADP potential make similar predictions for dislocation nucleation at a crack-tip. These results therefore validate the modeling procedure used in this paper, as detailed in section 2.

In the case of the present simulations, the distribution of stresses ahead of the crack-tip deviates from LEFM past a certain distance ahead of the crack-tip. When a dislocation is nucleated and exits the crack-tip region, it will interact with a stress field that is not representative of a realistic macroscopic system. This dislocation exerts an additional force on the crack-tip, which might affect the nucleation and movement of future dislocations. Therefore, in order to establish whether the size of the system plays a role in the effect precipitates have on crack-tip plasticity in this particular material system, additional simulations were conducted with two crystal dimensions: 100 $\times$ 100 $\times$ 20 nm, and 125 $\times$ 125 $\times$ 20 nm. For both sizes, a pristine system was created with crystal orientation B. The position of the leading dislocation after its nucleation from the crack-tip was calculated, and has been plotted in figure 4. Each curve corresponds to a different crystal size. The position of the dislocation starts from 0 nm, corresponding to the position of the crack-tip, and increases as it moves away towards the boundaries of the box. Observation of this figure shows that the behavior of the leading dislocation is the same for all crystal sizes up to 0.5% strain (deformation past initial nucleation); past this level of deformation, the curves start diverging as the leading dislocation starts interacting with the boundary of the smaller boxes. In the 100 nm box, the leading dislocation interacts with the boundary at 0.5% strain; in the 125 nm, this interaction starts at 0.6% strain. When the leading dislocation starts interacting with the crack-tip, its distance from the crack-tip does not increase anymore, and starts fluctuating. This behavior is not representative of a macroscopic system, in which the leading dislocation would continue moving away from the crack-tip with increasing crystal deformation. It is therefore clear from this plot that the behavior of a larger system is closer to that of an infinite crystal. Furthermore, the position of the leading dislocation can be considered a useful metric to describe the evolution of plasticity ahead of the crack-tip as it is largely independent of crystal size, provided that the leading dislocation is not interacting with the system's boundaries.

In figure 5(a), the position of the leading dislocation nucleated in crystal orientations A and B has been plotted in terms of the applied strain past the nucleation of the first dislocation.

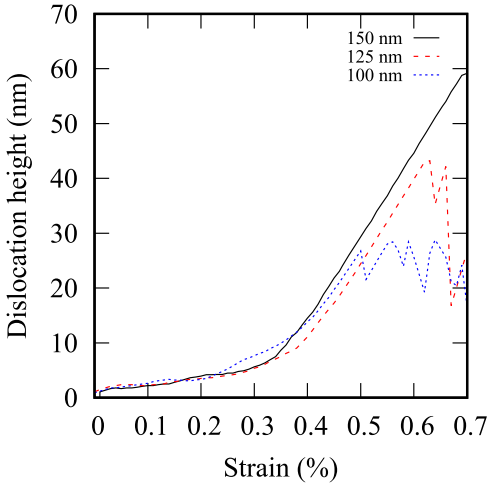

Figure 4. Effect of crystal size on the height of the leading dislocation in orientation B. The strain corresponds to the amount of deformation of the box after the nucleation of the first dislocation.

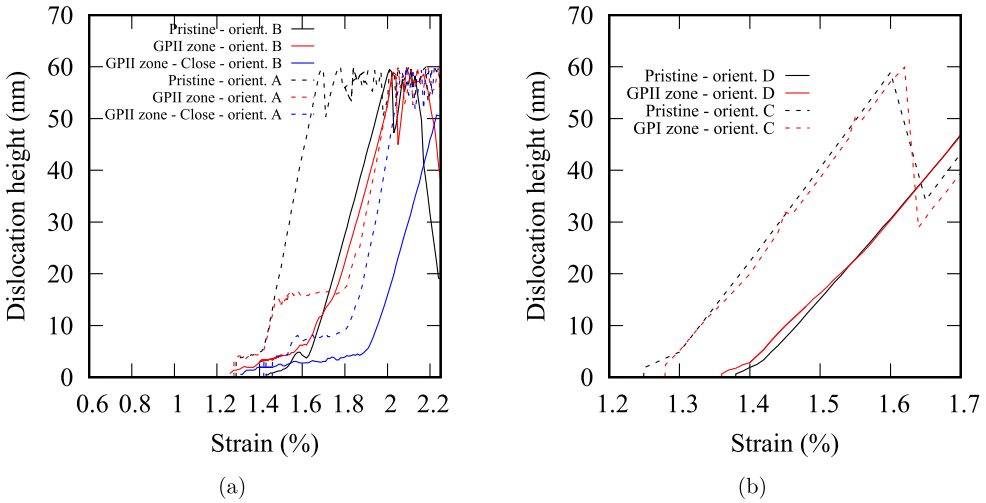

Figure 5. (a) Leading dislocation height in simulation box for crystal orientations A and B. (b) Dislocation height for crystal orientations C and D. The strain corresponds to the amount of deformation of the box after the nucleation of the first dislocation.

In the case of crystal orientation A, the dislocations were nucleated on the $(11\bar{1})$ plane oriented at 70.53° relative to the plane of the crack. All dislocations emitted from the crack-tip are [112] Shockley partials in crystal orientation A, as identified using the crystal analysis tool [40]. In the case of crystal orientation B, two slip systems were available, on the (111) and $(11\bar{1})$ planes, oriented at 35.26° relative to the plane of the crack. No complementary partials were nucleated in these crystal orientations, and as additional dislocations were nucleated with increased loading, the crack-tip became more blunt. Moreover, the crack grew with increasing loading, and at each atomic increment in crack size, further Shockley partials were

nucleated on the newly available slip planes, leading to further twin thickening. This effect has been discussed by Andric and Curtin [19]. From figure 5(a), it can be seen that for crystal orientation A, the precipitate (a 10 nm GPII zone) located 100 Å from the crack-tip has a negligible effect on the nucleation strain of the first dislocation. This suggests that even though the precipitate is quite large, its effect on the evolution of stress along the crack-tip prior to the onset of plasticity is not very strong. In the case of crystal orientation B, the first dislocation of the pristine system was nucleated at 1.23% strain on the (111) plane; the second dislocation was nucleated at approximately 1.45% strain on the $(11\bar{1})$ slip plane. In the reinforced system, the first dislocation was nucleated at 1.26% strain on the $(11\bar{1})$ plane, and the second at 1.48% strain on the (111) plane. These slight effects might be due to the precipitates.

Initially, in crystal orientation A, the position of the leading dislocation is the same in the pristine and reinforced systems (when the precipitate is located 100 Å from the crack-tip). When the applied strain is increased, the results between the pristine and the reinforced system start diverging, and the leading dislocation is pinned by the precipitate for a while, before overcoming it and moving towards the boundaries of the box, as shown by the dotted lines in figure 5(a). For crystal orientation B, when the precipitate is located 100 Å from the crack-tip, the initial behavior of the leading dislocation on the $(11\bar{1})$ slip plane is slightly different from a pristine system, however, after 1.6% strain, the behavior of both systems is the same. This suggests that the precipitate in this particular configuration has a negligible effect on the position of the leading dislocation.

In order to further quantify the effect of precipitates on crack-tip plasticity, two additional simulations for crystal orientations A and B were conducted, whereby a precipitate was placed 10 Å away from the crack-tip. In this region, the stress distribution is largely dominated by the K_I field of the crack-tip. The results are also shown in figure 5(a). Interestingly, the first dislocation is nucleated later in crystal orientation A: 1.42% instead of 1.3%. In crystal orientation B, the leading dislocation is nucleated slightly later relative to a system with a precipitate 100 Å away from the crack-tip. This suggests that the precipitates have an effect on dislocation nucleation when they are sufficiently close to the crack-tip that their residual stress fields affect the crack-tip. The leading dislocation then interacts with the precipitate in both crystal orientations and does not move as far away from the crack-tip. Past a certain amount of crystal deformation, however, the dislocation overcomes the precipitate and reaches the boundary of the box. It can be concluded that a precipitate closer to the crack-tip inhibits plasticity more strongly in these two crystal orientations.

Visual inspection of the microstuctures confirmed that the first dislocation was closer to the crack-tip in the reinforced systems relative to a pristine crystal due to its interaction with the precipitate. This was found to prevent the nucleation of additional dislocations, showing that the precipitates affect crack-tip plasticity. This shielding effect suggests that the stress field induced by the dislocations dominates the response of the crack-tip, whereas the residual stress field around the Cu precipitate does not affect stress distribution at the crack-tip very significantly prior to the nucleation of the first dislocation. The negligible effect of the precipitate on dislocation nucleation when it is located 100 Å from the crack-tip can be rationalized based on Eshelby's inclusion theory [42], whereby the stress field induced by a coherent inclusion in a linear elastic matrix decays at the rate of $1/r^2$. Therefore, the effect of a precipitate on dislocation nucleation is negligible past a small distance. In summary, for crystal orientations A and B, the precipitates inhibit crack-tip plasticity by pinning the first dislocation. These results are a significant finding for the AlCu alloy system, as they provide a direct explanation for the reduction in ductility with increasing precipitate volume fraction.

In crystal orientation C, dislocations were nucleated on the $(11\bar{1})$ planes oriented at 50.77° relative to the loading axis. The Burgers vector for all dislocation was given by: $b_p = \frac{a_0}{2}[011]$; the dislocations were made up of two Shockley partials separated by a small intrinsic stacking fault. In the case of crystal orientation D, the same mechanism of plastic deformation was observed, however the slip plane was oriented at 39.23° instead. In figure 5(b), the position of the leading dislocation in crystal orientations C and D has been plotted: the behavior is very similar in both cases, and clearly dislocation nucleation is not at all affected by the precipitates in this range of applied strains. The leading dislocation barely interacts with the precipitate, in contrast to crystal orientations A and B, thereby moving out of the crack-tip region unimpeded. Note that the slightly different nucleation strains between pristine and reinforced systems are due to the smaller number of snapshots used for the simulations without a precipitate, which precluded a precise comparison of the dislocation nucleation strains. Finally, we should note that the effect of orientation on the type of defect nucleated from the crack-tips (micro-twins versus full dislocations consisting of two Shockley partials and a thin stacking fault) is in agreement with the atomistic study by Yamakov *et al* [9]; this effect can be rationalized based on the orientation of the Burgers vectors of the dislocations relative to the loading direction.

3.3. Interaction of crack-tip nucleated dislocations with precipitates

In the previous section, the effect of a precipitate located either 100 or 10 Å from the crack-tip on dislocation nucleation was investigated. The planar Cu GPI zone lay in the (001) plane of the crystal. For the micro-twin moving along the $(11\bar{1})$ slip plane in the first crystal orientation, the mechanism for the dislocation-precipitate interaction between the micro-twin nucleated at the crack-tip and the GPII zone is shown in figures 6(a) and (b). The figure shows representations of the dislocations using the common neighbor analysis. Only atoms that are not in their regular FCC arrangement are shown, which include the crack faces. Initially, the micro-twin is comprised of 3 adjacent partial dislocations with the same [112] Burgers vector. The interaction between the dislocations and the precipitate has several stages. At first, the first dislocation approaches the GPII zone and bows around it due to the local misfit stress field, thereby adopting a local screw orientation. Thereafter, it cross-slips onto the three adjacent slip planes ($(\bar{1}11)$, $(1\bar{1}1)$ and (111)), creating stair-rod dislocations at the intersection of the {111} slip planes. Eventually, the dislocation cuts the precipitate, leaving behind a dislocation network of partials and stair-rods around the particle because of the partial cross-slip. Even though the dislocations bow significantly around the GPII zone, inspection of the precipitate after the interaction showed no dislocation loop. Moreover, the precipitate was cut at the location of the slip plane of the dislocations. In the case of crystal orientation B, a very similar mechanism of interaction was found, but no cross-slipping was observed, presumably because of the orientation of the potential slip planes relative to the loading axis.

In the case of crystal orientations C and D, the first full dislocation nucleated from the crack-tip interacted with the GPII zone in the same way as reported by Singh and Warner [25] for an uncracked Al crystal with a pre-existing dislocation: leading partial cutting, and trailing partial looping. This interaction mechanism is illustrated in figures 6(c) and (d). Visualization of the GPII zone following the interaction showed that the precipitate had been sheared across the slip plane of the dislocations. In the case of crystal orientation C, the second dislocation emitted from the crack-tip interacted with the GPII zone differently: a sessile defect was nucleated when the dislocation reached the precipitate, preventing the dislocation from moving forward. This behavior has been observed before by Singh and Warner [25] in the case where the dislocation was slightly offset with respect to the midsection of the GPII zone.

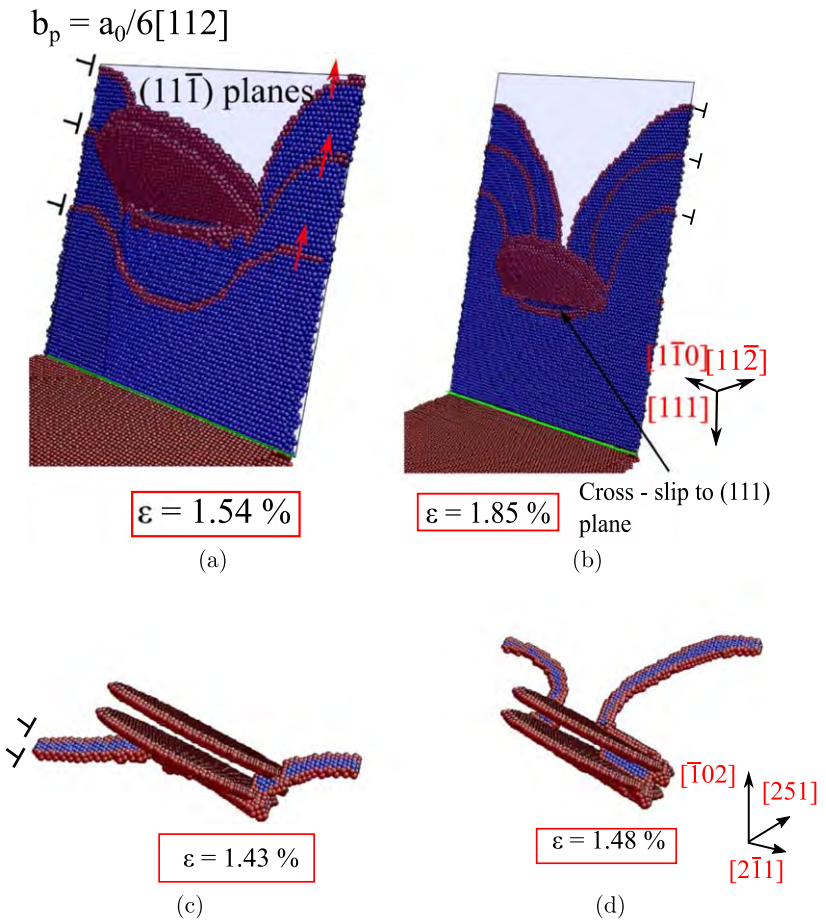

Figure 6. Interaction mechanism between dislocations nucleated from the crack-tip and a 10 nm GPII zone in crystal orientation A ((a) and (b)) and crystal orientation D ((c) and (d)).

It was argued in that work that this sessile defect is an athermal artifact, and was not seen at higher temperatures. Therefore, results for this simulation will not be discussed further. Instead, the analysis for crystal orientation C will focus on a 6 nm GPI zone. Lastly, in the case of crystal orientation D, subsequent dislocations underwent limited cross-slip around the precipitate. This interaction is shown in figure 7. The cross-slip mechanism led to the appearance of a jog on the dislocation; once the dislocation overcame the precipitate, a row of vacancies was created until the jog was annihilated. This partial cross-slip of the dislocation might have been enabled by the orientation of the primary slip plane relative to the loading direction of the crystal, as well as the position of the slip plane relative to the mid-plane of the precipitate. The next dislocations interacted with the precipitate in a similar manner, leading to a large number of dislocation defects around the precipitate. This mechanism of interaction is illustrated in figure 7.

The interaction time between the first dislocation and the GPII zone in each crystal orientation has been plotted in figure 8. In crystal orientation A, where the slip plane is oriented at 70.53° relative to the loading direction induced the longest interaction at

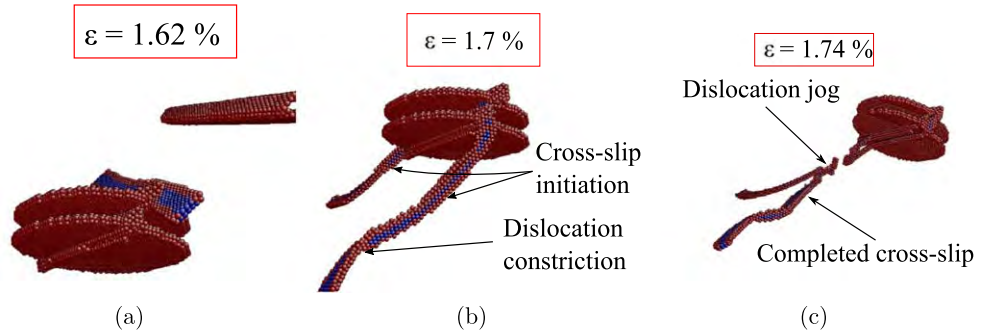

Figure 7. Interaction mechanism between the second full dislocation nucleated from the crack-tip and a 10 nm GPII zone in crystal orientation D.

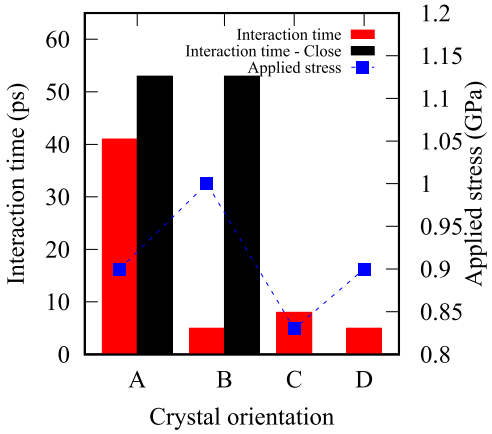

Figure 8. Dislocation-precipitate interaction time for each crystal orientation for the first dislocation, with a precipitate located either 10 or 100 Å away from the crack-tip.

approximately 53 ps for a precipitate 10 Å from the crack-tip, and 41 for a precipitate 100 Å away. In crystal orientation B, the precipitate had a negligible effect on the first dislocation when it was located 100 Å away from the crack-tip (with an interaction time of about 5 ps), but had a very large effect when it was located 10 Å away (with an interaction time of about 53 ps). In orientations C and D, the interaction was much shorter. Note that in these two orientations, the precipitate was always 100 Å from the crack-tip, as precipitates located closer to the crack-tip caused unphysical mechanisms of interaction. In order to understand these results, the applied stress at the point when the first dislocation meets the precipitate has also been plotted in the same figure. There is no clear correlation between the applied stress and the dislocation-precipitate interaction time. The applied stresses are very high, so the interaction time was instead most likely dependent on the interaction mechanism and the orientation of the crystal. The previous study by Singh and Warner [25] found that under athermal quasi-static loading conditions, depending on the orientation of the GP zone relative to the Burgers vector of the dislocation, the strengthening effect of a precipitate interacting

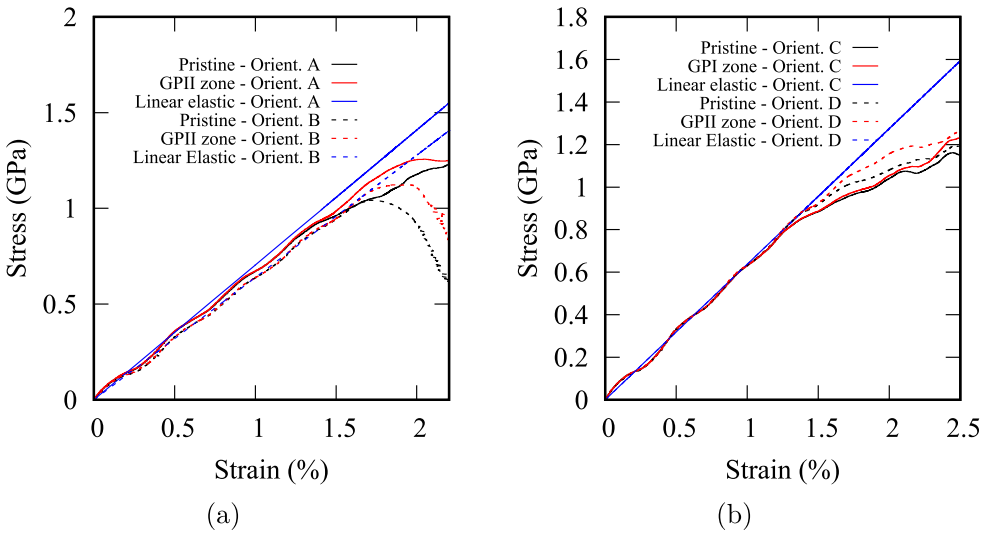

Figure 9. Stress–strain curves for the four crystal orientations, showing the effect of precipitates located on the slip plane.

with a full dislocation was between 185 and 270 MPa. In crystal orientations A and B, however, single Shockley partials are nucleated, instead of full dislocations. This different core structure leads to much stronger interaction with the precipitates.

While a GPII zone located 100 Å from the crack-tip did not have any significant effect on the first dislocation nucleation in any of the crystal orientations, it did change the evolution of the plasticity ahead of the crack-tip by slowing down the dislocations making up the micro-twin quite significantly. Shown in figure 9(a) are the stress–strain curves for the unreinforced and reinforced systems with crystal orientations A and B. As expected from the dislocation nucleation strains reported in the previous paragraphs, deviation from linear behavior in both systems becomes significant at 1.2% strain due to the nucleation and motion of dislocations. As the dislocations are moving away from the crack-tip, they cause stress relaxation for atoms on the slip plane due to the bond breaking and local plastic deformation. However, in the case of the reinforced system, the pinning of the micro-twin by the GPII zone leads to a larger stress as compared to the unreinforced system. The significant hardening effect induced by the precipitate affects the growth of the micro-twin and the overall plasticity ahead of the crack-tip. In the case of crystal orientation B, whose behavior is shown in the same plot, the precipitate also induces a larger stress due to its inhibiting effect on dislocation motion: the peak stress reaches 1.15 GPa versus 1.05 GPa for the unreinforced system. In the case of crystal orientations C and D (subplot (b)), where full dislocations are nucleated, the increase in flow stress induced by the precipitates is less significant. The lower interaction time (see figure 8) might explain this lower effect. However, it is also possible that the type of defect nucleated affects stress relaxation ahead of the crack-tip due to the different velocity of full dislocations relative to partial dislocations, as well as their different core structure. In summary, therefore, the volume-averaged behavior of crystal orientations C and D is not significantly affected by precipitates, in contrast to that of crystal orientations A and B.

4. Conclusion

In this study, we examined the role of nanoscale Cu precipitates on defect nucleation at the crack-tip and subsequent dislocation motion in cracked age hardened Al–Cu alloys using molecular dynamics. We investigated the role of GPII zones on the nucleation of Shockley partial dislocations from the crack-tip of an aluminum crystal. Nucleation of the first dislocation in the presence of a precipitate ahead of the crack-tip was not delayed significantly relative to a system without a precipitate, unless the precipitate was very close to the crack-tip. A micromechanical analysis of stress distributions around the crack-tip showed that the very localized nature of the misfit stress field of the precipitate explained this modest effect. However, the motion of the leading dislocation following its nucleation was strongly affected by the precipitate in crystal orientations A and B, where micro-twinning was dominant. In crystal orientations C and D, where full dislocations were nucleated, the precipitates had no effect on the motion of dislocations nucleated from the crack-tip in the range of applied strains that was considered.

The motion of the dislocations following nucleation and their interaction with precipitates was then examined. Due to the misfit stress field around the precipitate, and the nature of the loading conditions, cross-slip was observed in crystal orientation A when the nucleated defect interacted with a GPII zone, in combination with shear cutting. In crystal orientation B, similarly, shear cutting was observed, but without any cross-slipping. In the case of crystal orientations C and D, for which full dislocation slip was observed, the interaction mechanism was the same as reported by Singh and Warner [25] for an uncracked system with a pre-existing dislocation, namely a combination of cutting and Orowan looping, except that limited cross-slip also occurred, which led to the nucleation of dislocation jogs and trailing vacancies. These results were explained based on the orientation of the available slip systems relative to the applied loading direction.

The precipitates slowed down the dislocations quite significantly in crystal orientations A and B, but much less in orientations C and D. These differences might be due to the core structure of the defects and to the ensuing interaction mechanisms between dislocations and precipitates. The stress–strain curves plotted for each crystal orientation showed significant hardening for crystal orientations A and B, where micro-twinning was observed. In the case of crystal orientations C and D, where full dislocation slip was observed, the hardening effect was much more modest. These results suggest that the Machová core structure of the dislocation affects the constitutive behavior of the crystal quite significantly. Based on these results, it is concluded that nanometric precipitates in aluminum can under certain conditions appreciably inhibit crack-tip plasticity, and that the resistance they oppose to plastic deformation needs to be considered in future models of fracture toughness of aluminum–copper alloys to explain the transition from ductile to brittle behavior with increasing Cu concentration.

Acknowledgments

Computations were performed with support from Compute Canada super-computing facilities Scinet HPC consortium and the Shared Hierachical Academic Research Computing Network (Sharcnet). The authors gratefully acknowledge their support.

Financial support for this work was provided by the Natural Sciences and Engineering Research Council of Canada (NSERC) and the University of Toronto.

The authors declare no conflict of interest during the preparation of this manuscript.

ORCID iDs

Thomas Berton https://orcid.org/0000-0001-9647-2675
Chandra Veer Singh https://orcid.org/0000-0002-6644-0178

References

[1] Martin J W 1998 *Precipitation Hardening* (Oxford: Butteworth-Heinemann)
[2] Schwalbe K-H 1977 On the influence of microstructure on crack propagation mechanisms and fracture toughness of metallic materials *Eng. Fract. Mech.* **9** 795–832
[3] Yamakov V, Saether E, Phillips D R and Glaessgen E H 2006 Molecular-dynamics simulation-based cohesive zone representation of intergranular fracture processes in aluminum *J. Mech. Phys. Solids* **54** 1899–928
[4] Machová A, Spielmannová A and Hora P 2009 3D atomistic simulation of the interaction between a ductile crack and a Cu nanoprecipitate *Modell. Simul. Mater. Sci. Eng.* **17** 035008
[5] Cheng Y, Shi M X and Zhang Y W 2012 Atomistic simulation study on key factors dominating dislocation nucleation from a crack tip in two FCC materials: Cu and Al *Int. J. Solids Struct.* **49** 3345–54
[6] Terentyev D, Zhurkin E E and Bonny G 2012 Emission of full and partial dislocations from a crack in BCC and FCC metals: An atomistic study *Comput. Mater. Sci.* **55** 313–21
[7] Terentyev D and Gao F 2013 Blunting of a brittle crack at grain boundaries: an atomistic study in BCC iron *Mater. Sci. Eng.* A **576** 231–8
[8] Zhang J and Ghosh S 2013 Molecular dynamics based study and characterization of deformation mechanisms near a crack in a crystalline material *J. Mech. Phys. Solids* **61** 1670–90
[9] Yamakov V I, Warner D H, Zamora R J, Saether E, Curtin W A and Glaessgen E H 2014 Investigation of crack tip dislocation emission in aluminum using multiscale molecular dynamics simulation and continuum modeling *J. Mech. Phys. Solids* **65** 35–53
[10] Liu Z-G, Wang C-Y and Yu T 2013 Influence of Re on the propagation of a Ni/Ni 3 Al interface crack by molecular dynamics simulation *Modell. Simul. Mater. Sci. Eng.* **21** 045009
[11] Liu Z-G, Wang C-Y and Yu T 2015 Effect of Re on dislocation nucleation from crack tip in Ni by atomistic simulation *Comput. Mater. Sci.* **97** 127–35
[12] Baker K L and Warner D H 2014 An atomistic investigation into the nature of near threshold fatigue crack growth in aluminum alloys *Eng. Fract. Mech.* **115** 111–21
[13] Chakraborty S, Zhang J and Ghosh S 2016 Accelerated molecular dynamics simulations for characterizing plastic deformation in crystalline materials with cracks *Comput. Mater. Sci.* **121** 23–34
[14] Chandra S, Kumar N N, Samal M K, Chavan V M and Patel R J 2016 Molecular dynamics simulations of crack growth behavior in Al in the presence of vacancies *Comput. Mater. Sci.* **117** 518–26
[15] Rajan V P and Curtin W A 2016 Crack tip blunting and cleavage under dynamic conditions *J. Mech. Phys. Solids* **90** 18–28
[16] Shiari B and Miller R E 2016 Multiscale modeling of crack initiation and propagation at the nanoscale *J. Mech. Phys. Solids* **88** 35–49
[17] Petucci J, Leblond C and Karimi M 2014 Molecular dynamics simulations of brittle fracture in fcc crystalline materials in the presence of defects *Comput. Mater. Sci.* **86** 130–9
[18] Wang L, Liu Q and Shen S 2015 Effects of void-crack interaction and void distribution on crack propagation in single crystal silicon *Eng. Fract. Mech.* **146** 56–66
[19] Andric P and Curtin W A 2018 New theory for crack-tip twinning in fcc metals *J. Mech. Phys. Solids* **113** 144–61
[20] Andric P and Curtin W A 2017 New theory for mode I crack-tip dislocation emission *J. Mech. Phys. Solids* **106** 315–37
[21] Möller J J 2017 *Atomistic Simulations of Crack Front Curvature Effects and Crack-Microstructure Interactions* University of Erlangen-Nuremberg Doctoral Thesis
[22] Möller J J and Bitzek E 2014 Fracture toughness and bond trapping of grain boundary cracks *Acta Mater.* **73** 1–11

[23] Rice J R 1992 Dislocation nucleation from a crack tip: an analysis based on the Peierls concept *J. Mech. Phys. Solids* **40** 239–71
[24] Buze M, Hudson T and Ortner C 2018 *Analysis of an atomistic model for anti-plane fracture*
[25] Singh C V and Warner D H 2010 Mechanisms of Guinier-Preston zone hardening in the athermal limit *Acta Mater.* **58** 5797–805
[26] Granberg F, Terentyev D, Henriksson K O E, Djurabekova F and Nordlund K 2014 Interaction of dislocations with carbides in BCC Fe studied by molecular dynamics *Fusion Sci. Technol.* **66** 283–8
[27] Bacon D J, Osetsky Y N and Rodney D 2009 Dislocation-obstacle interactions at the atomic level *Dislocations in Solids* vol 15 (Amsterdam: Elsevier) pp 1–90
[28] Singh C V and Warner D H 2013 An atomistic-based hierarchical multiscale examination of age hardening in an Al-Cu alloy *Metall. Mater. Trans.* A **44** 2625–44
[29] Singh C V, Mateos A and Warner D H 2011 Atomistic simulations of dislocation-precipitate interactions emphasize importance of cross-slip *Scr. Mater.* **64** 398–401
[30] Olmsted D L, Hector L G and Curtin W A 2006 Molecular dynamics study of solute strengthening in Al/Mg alloys *J. Mech. Phys. Solids* **54** 1763–88
[31] Kocks U F, Argon A S and Ashby M F 1975 Thermodynamics and Kinetics of Slip *Progress in Materials Science* (Oxford: Pergamon)
[32] Leyson G P M, Curtin W A, Hector L G and Woodward C F 2010 Quantitative prediction of solute strengthening in aluminium alloys *Nat. Mater.* **9** 750–5
[33] Liu T and Groh S 2014 Atomistic modeling of the crack-void interaction in α-Fe *Mater. Sci. Eng.* A **609** 255–65
[34] Plimpton S 1995 Fast parallel algorithms for short-range molecular dynamics *J. Comput. Phys.* **117** 1–19
[35] Byrne J G, Fine M E and Kelly A 1961 Precipitate hardening in an aluminium-copper alloy *Phil. Mag.* **6** 1119–45
[36] Cai J and Ye Y 1996 Simple analytical embedded-atom-potential model including a long-range force for fcc metals and their alloys *Phys. Rev.* B **54** 8398–410
[37] Apostol F and Mishin Y 2011 Interatomic potential for the Al–Cu system *Phys. Rev.* B **83** 1–8
[38] Li J 2003 AtomEye: an efficient atomistic configuration viewer *Modell. Simul. Mater. Sci. Eng.* **11** 173–7
[39] Faken D and Jonsson H 1994 Systematic analysis of local atomic structure combined with 3D computer graphics *Comput. Mater. Sci.* **2** 279–86
[40] Stukowski A and Albe K 2010 Extracting dislocations and non-dislocation crystal defects from atomistic simulation data *Modell. Simul. Mater. Sci. Eng.* **18** 085001
[41] Ringdalen Vatne I, Stukowski A, Thaulow C, Østby E and Marian J 2013 Three-dimensional crack initiation mechanisms in bcc-Fe under loading modes I, II and III *Mater. Sci. Eng.* A **560** 306–14
[42] Eshelby J D 1957 The determination of the elastic field of an ellipsoidal inclusion, and related problems *Proc. R. Soc.* A **241** 376–96